



Effect of Zr/Ti Ratio on the Structure and Electrical Properties of $0.7\text{PbZr}_x\text{Ti}_{1-x}\text{O}_3$ - $0.3\text{Pb}(\text{Zn}_{1/3}\text{Nb}_{2/3})\text{O}_3$ Piezoelectric Ceramics

Cong Yang^{1,2} · Jianzhou Du^{1,2,3} · Yuansheng Chen¹ · Yunping Li¹ · Jingyi Yan² · Luming Wang¹ · Kongjun Zhu³

Received: 30 November 2023 / Accepted: 22 February 2024 / Published online: 13 March 2024
© The Minerals, Metals & Materials Society 2024

Abstract

Ternary system piezoelectric ceramics $0.7\text{PbZr}_x\text{Ti}_{1-x}\text{O}_3$ - $0.3\text{Pb}(\text{Zn}_{1/3}\text{Nb}_{2/3})\text{O}_3$ (abbreviated as 0.7PZT_x - 0.3PZN) were prepared by a traditional solid-phase process. With the increase in Zr content, the electrical properties of the ceramics were significantly improved, and this result could be attributed to the change in the ceramic phase structure. The relationship between the change in Zr content and the ceramic phase structure and properties was investigated in detail by component modulation. X-ray diffraction (XRD) analyses showed that the phase structure of the ceramics undergoes a transition from the coexistence of tetragonal (T) and rhombohedral (R) phases to the predominance of rhombohedral (R) phases as the Zr content x increases. The phase structure of the ceramics at $x=0.49$ is closer to the morphotropic phase boundary (MPB), with about 32% of the T-phase and 68% of the R-phase, and possesses good electrical properties: $d_{33}=483$ pC/N, $k_p=0.69$, $\varepsilon_r=2171.7$, $\tan\delta=0.016$, $T_c=292.5^\circ\text{C}$, $P_r=35.9$ $\mu\text{C}/\text{cm}^2$, $E_c=7.7$ kV/mm. Constructing the MPB of 0.7PZT - 0.3PZN piezoelectric ceramics by varying the Zr content can be effective in improving the electrical properties and understanding more broadly how the change in Zr/Ti composition affects the piezoelectric behavior.

Keywords PZT-PZN · piezoelectric ceramics · MPB · electrical properties

Introduction

The binary piezoelectric ceramic lead zirconate titanate ($\text{PbTi}_{1-x}\text{Zr}_x\text{O}_3$, abbreviated as PZT) is an important functional material widely used in structural health inspection, energy harvesting, piezoelectric sensing, and actuation,^{1–4} due to its superior dielectric and piezoelectric properties. With the rapid development of the electronic information industry, electronic components are required to be miniaturized, high-performance, and highly reliable. Therefore, there is growing interest in adding other components to PZT ceramics to form higher-performance ternary or multisystem PZT-based piezoelectric ceramics, especially

relaxor ferroelectrics with high dielectric constants and diffuse phase transition properties, such as $\text{Pb}(\text{Mg}_{1/3}\text{Nb}_{2/3})\text{O}_3$ (PMN), $\text{Pb}(\text{Ni}_{1/3}\text{Nb}_{2/3})\text{O}_3$ (PNN), and $\text{Pb}(\text{Zn}_{1/3}\text{Nb}_{2/3})\text{O}_3$ (PZN), and typical ternary system relaxation ferroelectric ceramics such as PMN-PZT,^{5–7} PZN-PZT,^{8–10} and PNN-PZT.^{11–13}

Numerous studies have found that the optimal electrical properties are obtained when the ceramic composition is close to the morphotropic phase boundary (MPB) region, which is a critical domain for the coexistence of different ferroelectric phases (e.g., rhombohedral and tetragonal phases).^{14–16} $\text{Pb}(\text{Zr}_x\text{Ti}_{1-x})\text{O}_3$ ceramics are coexisting tetragonal and monoclinic phases in the MPB and exhibit excellent dielectric, elastic, and piezoelectric properties.¹⁷ Therefore, the construction of the MPB of PZT ceramics can be improved by component modulation, ion doping, and process optimization to improve its electrical properties. Ta_2O_5 was used as a donor dopant to construct the rhombohedral-tetragonal (R-T) MPB of PNN-PZT ceramics, resulting in ultrahigh piezoelectric (1090 pC/N) and inverse piezoelectric (1493 pm/V) coefficients.¹⁸ In a study wherein PSN content was varied to construct MPB of $y\text{PSN}$ - 0.3PNN - $(0.7-y)\text{PZT}$ ceramics,¹⁹ as the PSN content increased, the

✉ Jianzhou Du
dujianzhou123@163.com

¹ Yancheng Institute of Technology, Yancheng 224051, People's Republic of China

² Jiangsu Dongpu Fine Ceramic Technology Co. Ltd., Lianyungang 222000, People's Republic of China

³ College of Materials Science and Technology, Nanjing University of Aeronautics and Astronautics, Nanjing 210016, People's Republic of China

MPB shifted to PT-rich regions, and the optimal electrical characteristics of 0.015PSN-0.3PNN-0.685PZT were found to be $d_{33} = 660 \text{ pC/N}$, $k_p = 0.68$.

PZN is a classic relaxation ferroelectric with a high Curie point ($T_C = 140^\circ\text{C}$) and large dielectric constant ($\epsilon_{\text{max}} = 22000$); incorporating PZN and PZT together forms a piezoelectric ceramic with a perovskite structure, which has the advantages of high density, good insulation, and good piezoelectric properties.²⁰ By adjusting the content of the relaxor ferroelectric PZN to construct the MPB of ceramics, the systems with better properties are mostly 0.8PZT-0.2PZN and 0.7PZT-0.3PZN, whose phase structure coexists in tripartite and tetragonal phases. The increase in PZN content favors the relaxation behavior, and some researchers have prepared PZT-PZN ceramic fractions with piezoelectric properties up to ($d_{33} = 550 \text{ pC/N}$, $k_p = 0.69$)²¹ and ($d_{33} = 690 \text{ pC/N}$, $k_p = 0.7$)²² at the MPB region. The Zr/Ti ratio determines the phase distribution of a ceramic. Changing the Zr/Ti ratio adjusts the ratio of the R-phase to the T-phase to construct the MPB of the ceramic and optimize its properties.²³ Doping modification by introducing trace additives near the MPB of PZN-PZT can further improve the properties of the ceramics. Wang et al.²⁴ proposed the use of La to dope 0.25PZN-0.75PZT and changed the Zr/Ti ratio to obtain the optimal electrical properties for the sample at Zr/Ti = 53/47: $d_{33} = 570 \text{ pC/N}$, $k_p = 0.6$. Varying the sintering temperature can also construct the MPB of PZT-PZN ceramics, which not only promotes grain growth but also enhances the ferroelectric and piezoelectric properties.²⁵

The solid solution PZT-PZN piezoelectric ceramics composed of PZT with ferroelectric properties and PZN with relaxation properties have high Curie temperatures and good electrical properties, while higher piezoelectric properties can be obtained by tuning the ceramic components to the vicinity of the MPB, so the phase-content relationship between the tetragonal and monoclinic phases can be adjusted by changing the Zr content. In this work, the system chosen was $0.7\text{PbZr}_x\text{Ti}_{1-x}\text{O}_3-0.3\text{Pb}(\text{Zn}_{1/3}\text{Nb}_{2/3})\text{O}_3$, and a detailed structural analysis of the system was carried out by varying the value of x . The work is devoted to constructing the morphotropic phase boundary of ceramics by changing the Zr content to obtain good piezoelectric properties. The effect of the change in Zr content on the change in the phase content of the ceramic MPB was investigated in detail, which will help to better explore how the change in phase content affects the electrical properties of the ceramics.

Experimental Procedure

In this experiment, $0.7\text{PbZr}_x\text{Ti}_{1-x}\text{O}_3-0.3\text{Pb}(\text{Zn}_{1/3}\text{Nb}_{2/3})\text{O}_3$ ternary piezoelectric ceramics were fabricated by the conventional solid-phase sintering process. The selected

pharmaceutical raw materials were analytical pure level PbO (99%), ZrO_2 (99%), TiO_2 (99.9%), Nb_2O_5 (99.5%), and ZnO (99.97%), and were weighed according to the stoichiometric ratio. The weighed raw materials with appropriate amounts of agate balls and anhydrous alcohol were put into a QM-3SP2 planetary ball mill for the first mixing and ball milling at a speed of 120 r/min for 12 h. The ball-milled powder was dried in a DL-101 constant-temperature drying oven at 80°C , then ground and sieved to obtain a powder with a certain particle size. The pre-pressed powder was sealed in a crucible and burned in an SG-XL1400 muffle furnace at 1050°C for 4 h. The second ball milling was carried out using the same method as the first ball milling in order to obtain a homogeneous powder and the desired particle fineness. After drying, polyvinyl alcohol (PVA) at a concentration of 5% was added as a binder for granulation, and the fine powdered material was aggregated into larger particles by passing through a 100 mesh sieve. The powder was pressed under pressure of 100 MPa to form a ceramic billet with a certain shape and density. The ceramic disks were sealed in a crucible and sintered, first at 200°C to remove moisture, then at 800°C and held for 4 h to remove PVA. The ceramic disks were covered with pre-fired powder, sealed in a crucible, and sintered at 1200°C for 2 h to obtain the final ceramic samples. The ceramic samples were sandpapered to 0.8 mm, brushed with silver paste, and dried. The ceramic samples were polarized in silicone oil for 30 min at 50°C with a DC field of 2 kV/mm. Finally, the samples were tested and analyzed for their properties after 24 h of resting.

A Bruker D8 Advance x-ray diffractometer was used to analyze the phase structure composition of the ceramics. Scanning electron microscopy (SEM; JEOL JMS-5610LV) was used to observe the microscopic surface of the ceramics. The mass of the ceramics was weighed with a German BS210S analytical balance, and the density was determined by the Archimedes drainage technique. A ZJ-3A d_{33} measuring instrument (Institute of Acoustics, Chinese Academy of Sciences) was used to measure the quasi-static piezoelectric constants at room temperature. The electromechanical coupling coefficients (k_p , k_{31}) and piezoelectric constants (d_{31}) were measured using an IEEE standard LCR analyzer based on the resonance and antiresonance methods. The relative dielectric constant (ϵ_r) and loss ($\tan\delta$) were measured using an HP4294A Precision Impedance Analyzer (Keysight/Agilent, Japan). The dielectric temperature characteristics of the ceramics were analyzed using the GJW-I dielectric temperature test system. The hysteresis lines of the ceramics were measured using the aixACCT TF 2000 ferroelectric analyzer (aixACCT Systems, Germany).

Results and Discussion

Electrical Properties

Figure 1 shows the electrical properties of 0.7PZT x -0.3PZN ceramics at room temperature. As the Zr content x increases from 0.45 to 0.49, the d_{33} and k_p values show an increasing trend, with d_{33} achieving a maximum value of 483 pC/N and k_p of 0.69 at $x=0.49$. As the Zr content x increases further to 0.51, the d_{33} value begins to decrease to 405 pC/N, while k_p achieves a maximum value of 0.70, as shown in Fig. 1a. The trend of d_{31} is the same as d_{33} , and k_{31} is similar to k_p . It can be seen in Fig. 1b that d_{31} first increases with the increase in Zr content, reaches a maximum value of -214.9 pC/N at $x=0.49$, and then decreases, while k_{31} increases from 0.21 to 0.41. As shown in Fig. 1c, when the value of x increases from 0.45 to 0.47, ϵ_r increases drastically from 1518.7 to 2164, and then increases to 2127 when the value of x reaches

0.49. The change in the dielectric constant can therefore be seen as a result of the grain boundaries and grains acting together. Dielectric loss is the loss of energy within a dielectric body due to heat generation under the influence of an electric field. In general, dielectric losses are related to the motion of the domain walls, and when an applied electric field is present, there is an interaction between the domain walls, resulting in energy loss in the motion of the domain walls. As x increases from 0.45 to 0.51, the trend in $\tan\delta$ is relatively flat, at 0.016, 0.015, 0.016, and 0.018 respectively.

It can be seen that the optimal piezoelectric properties are exhibited by the ceramic samples with Zr content $x=0.49$. To determine why the piezoelectric properties of ceramics improve with increasing Zr content, and whether it is the cause of changes in the homogeneity, densification, porosity, and phase structure of the ceramic components, further analysis was conducted in greater detail.

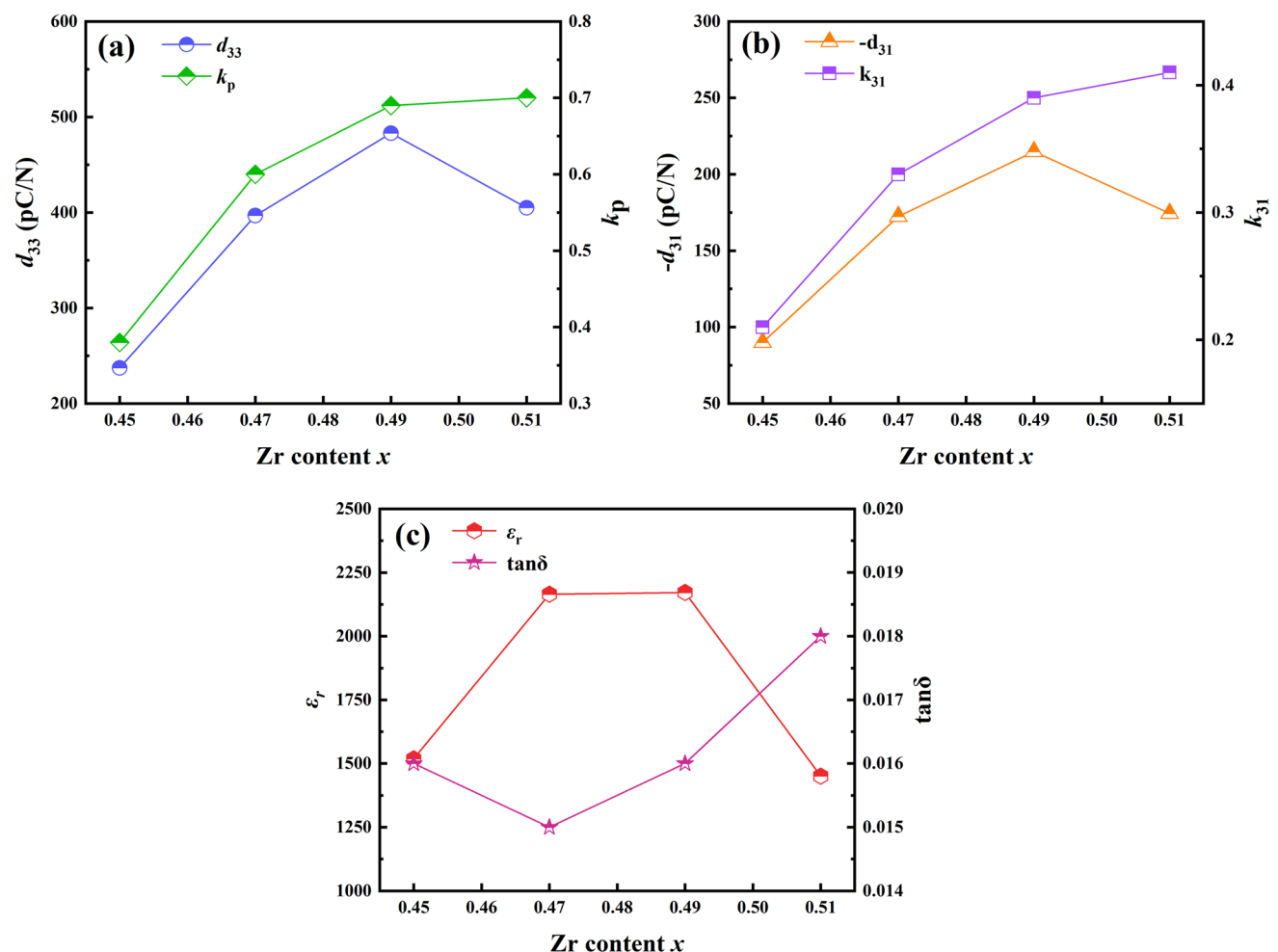


Fig. 1 The electrical properties of 0.7PZT x -0.3PZN ceramics measured at room temperature (a) d_{33} and k_p , (b) d_{31} and k_{31} , (c) ϵ_r and $\tan\delta$.

Phase Structure Analysis

The improvement in piezoelectric properties may be attributed to changes in the phase structure of the ceramics due to compositional variations; therefore, the phase structure of the 0.7PZT x -0.3PZN ceramics was analyzed by x-ray diffraction (XRD) patterns, as shown in Fig. 2. All ceramic samples exhibited a typical perovskite phase structure without the formation of other heterogeneous phases. In the range of 2θ from 20° to 70° , the diffraction peaks (111) did not split with increasing Zr content for any ceramic samples. On the contrary, in the samples with component $x \leq 0.49$, the (002) and (200) peaks, the (112) and (211) peaks, and the (202) and (220) peaks underwent significant splitting, suggesting that these piezoelectric ceramic structures are mainly tetragonal phase. When $x=0.51$, no splitting occurred in any of the peaks of this sample and there was only one peak, which indicates that the crystal structure of this component lattice is mainly a rhombohedral phase.

To analyze the phase structure changes of this ceramic in more detail, the XRD patterns at 43° – 46° were enlarged and the curves were separated using a Gaussian fitting function corresponding to the (002) peak of the tetragonal phase and the (200) peak of the rhombohedral phase, as shown in Fig. 2b–e. As the change in the peaks in the figure is not obvious, it can be seen that the phase structure changes from the tetragonal phase to the rhombohedral phase, while the proportion of each is not clear. Therefore, the simulated integral intensity of each peak was calculated to obtain the relative proportions of the tetragonal and rhombohedral phases in the phase structure. As shown in Fig. 2f, with increasing Zr content, the percentage of the rhombohedral phase increases, while the tetragonal phase shows the opposite trend. As x increases from 0.45 to 0.49, the tetragonal phase fraction decreases from 40% to 32% and the rhombic phase fraction increases from 60% to 68%. At $x=0.51$, only one peak is the predominantly rhombic phase. Thus, it can be summarized from Fig. 2 that the phase structure of this 0.7PZT x -0.3PZN ceramic undergoes a transition from a tetragonal phase to a rhombohedral phase as the Zr content increases, and the morphotropic phase boundary (MPB) lies between $x=0.49$ and 0.51. The associated results and changes are generally consistent with previous studies.²⁶

In the MPB region, where the ceramic structure exhibits a coexistence of rhombohedral and tetragonal phases, there are more possible directions of spontaneous polarization of the electric domains. The domains are easily oriented under the influence of the applied electric field, resulting in high piezoelectric properties for the ceramic. The piezoelectric constant d_{33} can reach its peak near the morphotropic phase boundary.²⁷ This precisely explains why the ceramic samples with Zr content x of 0.49 exhibited optimal piezoelectric properties in this experiment. Meanwhile, the

dielectric properties of ceramics are closely related to the microstructure of the ceramics, including grain size, density, and porosity.

Figure 3 shows the SEM images of 0.7PZT x -0.3PZN ceramics after sintering at 1200°C for 2 h. It can be seen that under the current sintering environment, the fracture mode of the ceramics is mainly along-crystal fracture, the grain size is mostly 2–8 μm , and all the samples can grow sufficiently, with small particles uniformly distributed around the large ones, and relatively dense microstructure. However, as the zirconium–titanium ratio increases, the grain size tends to increase slightly, as shown in Fig. 4, where the average particle size of all ceramic samples lies between 1.49 μm and 2.19 μm . Compared with the other samples, the sample with $x=0.51$ obtains the highest density, the most uniform grain size, and the tightest grain bonding. The change in grain size is an important factor influencing the dielectric properties of ceramics. Figure 5 shows the energy-dispersive x-ray spectroscopy (EDS) elemental diagrams of the 0.7PZT x -0.3PZN ceramic samples with different Zr content and the weight percentage of each element, with the major elements being Pb, Zr, Zn, Ti, Nb, and O. The Pb element accounted for the highest percentage by weight among all the samples, about 57%, whereas Zn had the lowest weight percentage, less than 5%. With the increase in Zr content, the ratio of Zr to Ti was 1.54, 1.87, 1.85, and 2.08, respectively, which was significantly increased. Generally, the relevant elements were distributed homogeneously at the micron scale.

The calculated densities of the ceramic samples all ranged from 7.86 to 8.24 g/cm^3 . Detailed data are shown in Table I, with small differences in density and shrinkage between the component samples. It can be deduced that near the morphotropic phase boundary, changes in the Zr content have little effect on density and shrinkage. As the Zr content increases, the density of the ceramic samples first increases and then decreases, with maximum density of 8235.8 kg/m^3 at Zr content $x=0.47$, after which it begins to decrease. The diameter shrinkage of all ceramic samples ranged from 0.12 to 0.132, with a minimum of 0.123 at Zr content $x=0.45$ and a maximum of 0.132 at $x=0.51$.

Dielectric Temperature Properties

The experimental data show that the grain size of the ceramics is positively correlated with the zirconium content, i.e., the greater the zirconium content, the larger the grain size. Since the dielectric constant is closely related to the grain size, the effect of different Zr content on the dielectric properties of 0.7PZT x -0.3PZN was analyzed, and the dielectric temperature variation characteristics of the ceramics were tested in the frequency range from 0.1 kHz to 1000 kHz, as shown in Fig. 6. It can be seen that at different test frequencies, the dielectric constant

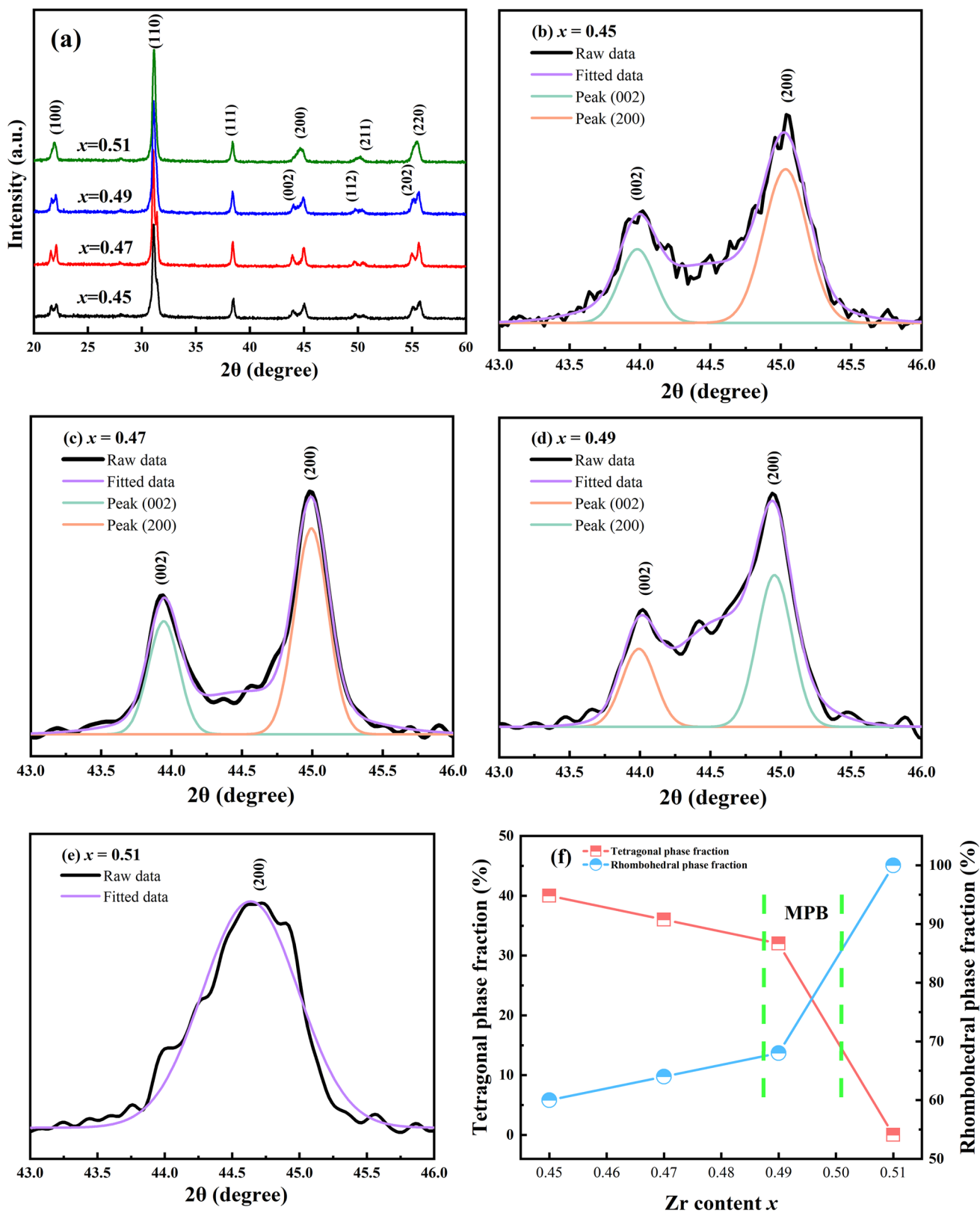


Fig. 2 (a) XRD patterns of 0.7PZTx-0.3PZN ceramics with various Zr content in the 2θ range of 20°–60°. Enlarged XRD pattern of 43°–46° diffraction peaks (b) x = 0.45, (c) x = 0.47, (d) x = 0.49, (e)

x = 0.51. (f) Variations in the relative content of the tetragonal and rhombohedral phase with different Zr content

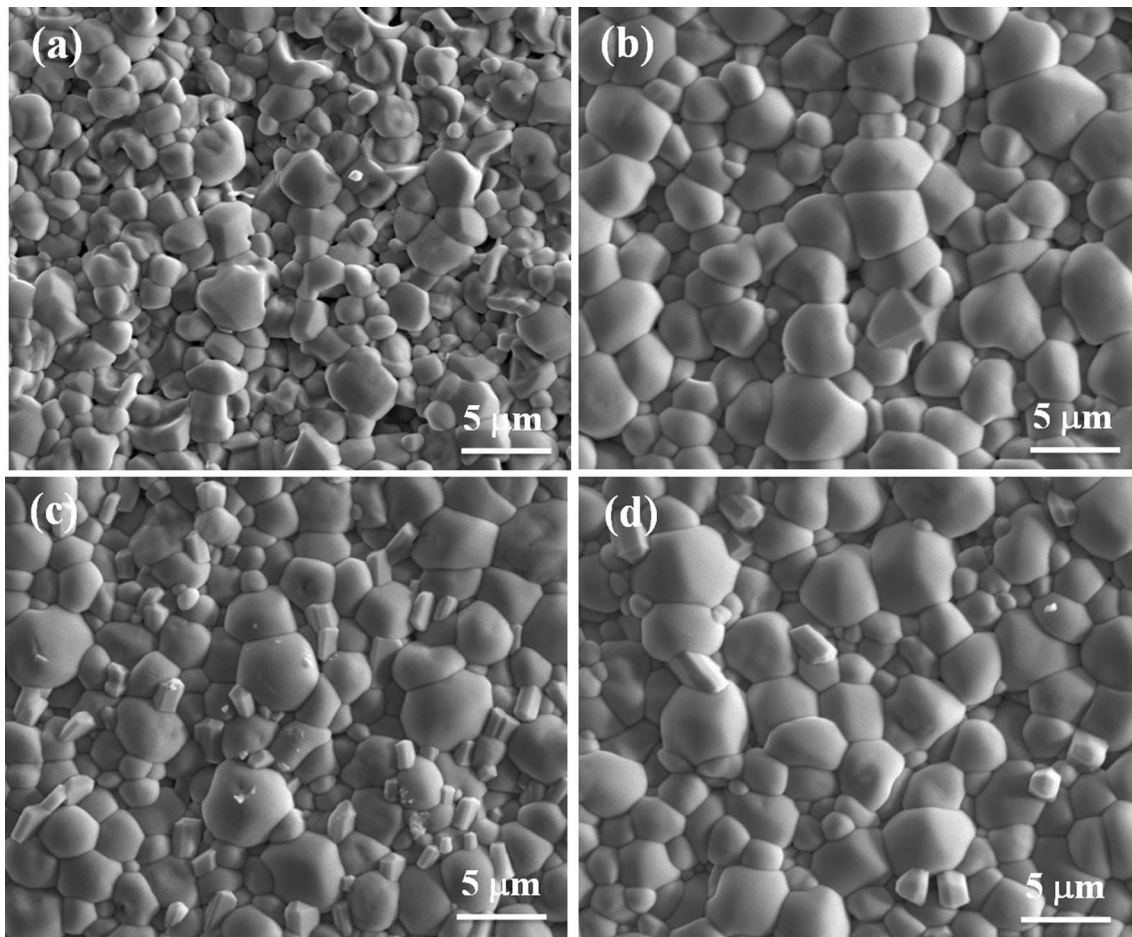


Fig. 3 SEM micrographs of 0.7PZTx-0.3PZN ceramics. (a) $x=0.45$, (b) $x=0.47$, (c) $x=0.49$, (d) $x=0.51$

shows a trend of increasing and then decreasing with the temperature change, and a region with width appears as the phase transition region of the ferroelectric phase to the paraelectric phase transition, and the temperature range of the change is roughly between 270°C and 310°C. As the frequency increases from 0.1 kHz to 100 kHz, the dielectric peak broadens and the value of the dielectric peak decreases. With the increase in the Zr content, the dielectric peaks move towards lower temperatures, while the corresponding values of the dielectric peaks increase significantly. The enhancement of the dielectric properties can be attributed to the increase in the grain size of the samples, making the domains easy to switch.²⁷ The dielectric loss in the low-temperature stage (0–250°C) shows a slightly decreasing trend. In the range from 250°C to 320°C, the dielectric loss increases and then decreases, and the dielectric loss appears to be the maximum value corresponding to the peak value, indicating that the phase transition occurs at this temperature. Finally, due to the free motion of carriers caused by high temperature, $\tan\delta$ increases rapidly.²⁸

The dielectric behavior of PZN–PZT, as a typical relaxed ferroelectric ceramic, can be explained using the Curie–Weiss law. The parameter γ can be seen as the degree of diffusion in terms of the relationship curve between $\ln(1/\epsilon_r - 1/\epsilon_m)$ and $\ln(T - T_m)$. At temperatures above T_m , the dielectric properties can be expressed in terms of a modified Curie–Weiss relationship as follows:

$$\frac{1}{\epsilon_r} - \frac{1}{\epsilon_m} = \frac{(T - T_m)^\gamma}{C} \quad (1 \leq \gamma \leq 2) \quad (1.1)$$

where ϵ_r is the dielectric constant at temperature T , ϵ_m is the maximum dielectric constant at the transition temperature (T_m), C is the Curie constant, and γ can be regarded as an index of the diffusion level. Values of γ ranging from 1 to 2 denote a normal ferroelectric to complete phase transition.²⁹ Figure 7a shows the curve of $\ln(1/\epsilon_r - 1/\epsilon_m)$ versus $\ln(T - T_m)$ for 0.7PZTx-0.3PZN ceramics evaluated at a frequency of 1 kHz. All the ceramic samples have relaxor properties but they are not significant, which indicates that changing the Zr content does not have a great effect on the

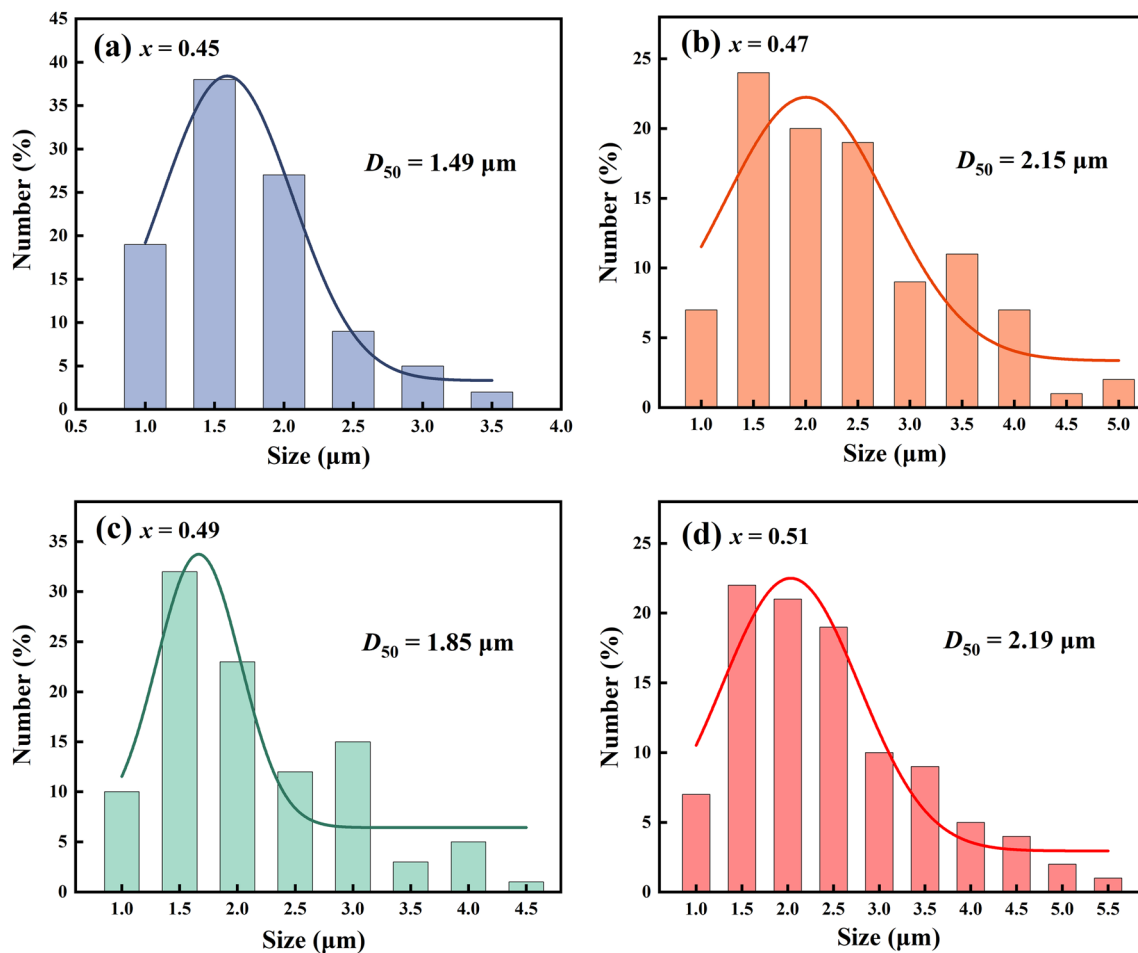


Fig. 4 Grain size distribution of 0.7PZTx-0.3PZN ceramics. (a) $x=0.45$, (b) $x=0.47$, (c) $x=0.49$, (d) $x=0.51$

relaxor properties of the ceramics. Figure 7b shows the γ values versus Curie temperature (T_c) for ceramic samples with different Zr content. As the Zr content increases, the γ value gradually decreases from 1.87 at $x=0.45$ to 1.7 at $x=0.51$. The trend of T_c is the same as γ , decreasing linearly from 306°C to 285°C.

Therefore, it can be concluded that the change in Zr content has little effect on the ceramic temperature in this system and the change in the dielectric temperature follows the law. The increase in the dielectric constant is attributed to the increase in ceramic grain size. Because the PZN content does not change, only changing the Zr content has no significant effect on the relaxation degree.

Ferroelectric Properties

Figure 8 displays the ferroelectric properties of 0.7PZTx-0.3PZN piezoceramics with $I-E$ curves and $P-E$ return at a frequency of 5 Hz and an electric field of 1.6 kV/mm. All components show the typical hysteresis lines of ferroelectrics with high symmetry and saturation, indicating that the

bias field of the samples is overcome by the applied electric field, and all have good ferroelectric properties. In addition, the current peak caused by the direction of the ferroelectric domains can be observed from the $I-E$ curve. With the increase in Zr content, P_r exhibits the same trend of growth as P_s , while the trend of E_c increases and then decreases, as shown in Table I. The values of P_s and P_r increased from 24.8 $\mu\text{C}/\text{cm}^2$ and 21.9 $\mu\text{C}/\text{cm}^2$ to 39.6 $\mu\text{C}/\text{cm}^2$ and 38.9 $\mu\text{C}/\text{cm}^2$, respectively, with the increase in Zr content $x=0.45$ to 0.51, while E_c achieves a maximum value of 10.9 kV/mm at Zr content $x=0.45$. The increase in the values of P_s and P_r may be explained by the fact that the increase in Zr content alters the crystal structure of the ceramics, thereby enhancing the likelihood of polarization. The results may also be influenced by the increase in grain size as well as the motion of the domain walls.⁹ Regarding E_c , it reaches its maximum value at Zr content of $x=0.45$. This may be linked to the specific interaction of the crystal structure with the Zr content at this point, creating an optimized environment that enables higher electric field strength to be reached at lower electric fields.

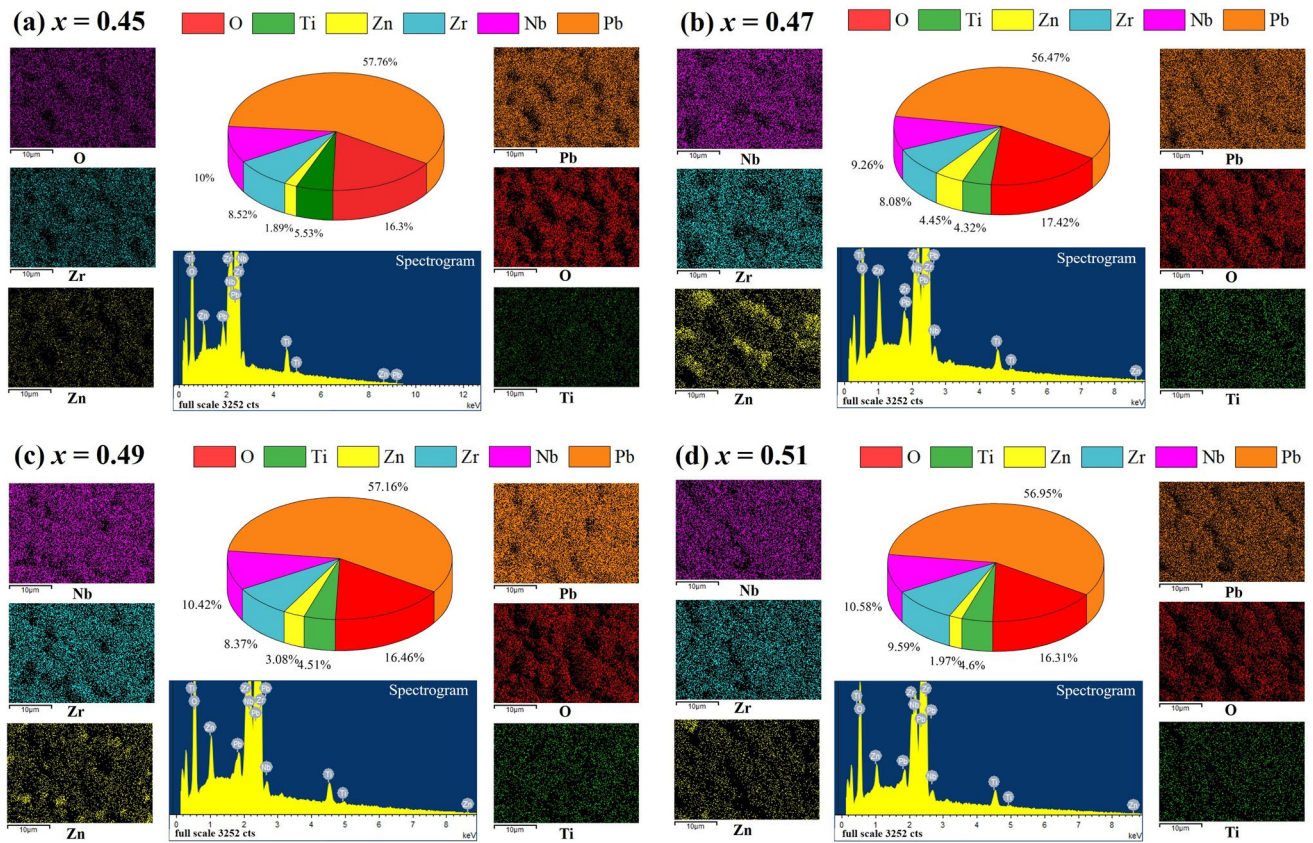


Fig. 5 The EDS elemental maps of 0.7PZTx-0.3PZN ceramic samples and the weight percentage of each element. (a) $x=0.45$, (b) $x=0.47$, (c) $x=0.49$, (d) $x=0.51$

Table 1 Details of the physical properties for 0.7PZTx-0.3PZN ceramics measured at room temperature

Composition	Density (kg/m^3)	d_{33} (pC/N)	k_p	ϵ_r	$\tan\delta$	T_c ($^\circ\text{C}$)	P_s ($\mu\text{C/cm}^2$)	P_r ($\mu\text{C/cm}^2$)	E_c (kV/mm)
$x=0.45$	7861.5	237.3	0.38	1518.7	0.016	306.2	24.8	21.9	10.0
$x=0.47$	8235.8	396.8	0.60	2164.9	0.015	300.0	37.8	34.8	10.9
$x=0.49$	8026.8	483	0.69	2171.7	0.016	292.5	38.1	35.9	7.7
$x=0.51$	8017.1	405	0.70	1450.6	0.018	285.8	39.6	38.9	6.5

From the I - E loops, it can be seen that all the components of the samples have distinct sharp current peaks in the vicinity of their respective coercive fields, which suggests that the ferroelectric domains are switched in response to the applied electric field. The switching current value increases significantly with increasing Zr content, which is caused by the construction of MPB that increases the amount of switchable ferroelectric domains and thus the activity.³⁰ In summary, the improved ferroelectric properties are attributed to the phase structure of the ceramics with the coexistence of tetragonal and tripartite phases, which are easily polarized to rotate in the MPB region.³¹

Conclusions

0.7PZTx-0.3PZN ceramics with Zr content of $x=0.45$ – 0.51 were fabricated via the traditional solid-phase reaction process. The Zr/Ti ratio plays a crucial role in determining the distribution of the ceramic phase structure. An increase in Zr content leads to a higher proportion of the monoclinic phase, while a decrease in Ti content results in a reduction in the tetragonal phase. As the morphotropic phase boundary represents a state where the tripartite and tetragonal phases coexist, it is more conducive to the polarization process, allowing

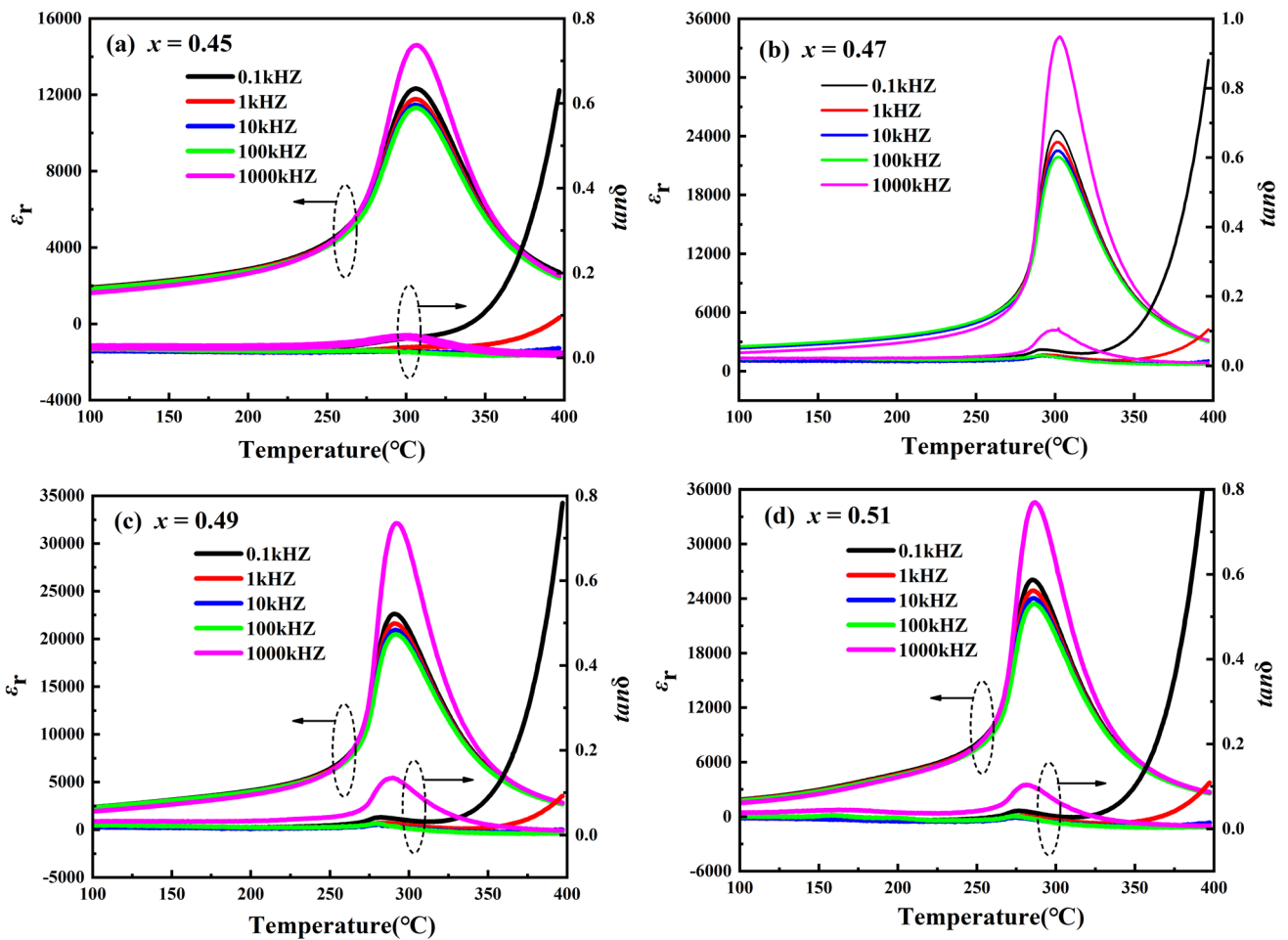


Fig. 6 The temperature and frequency dependence of relative dielectric constant (ϵ_r) and dielectric loss ($\tan\delta$) for the 0.7PZTx-0.3PZN piezoceramics with different Zr content: (a) $x = 0.45$, (b) $x = 0.47$, (c) $x = 0.49$, (d) $x = 0.51$.

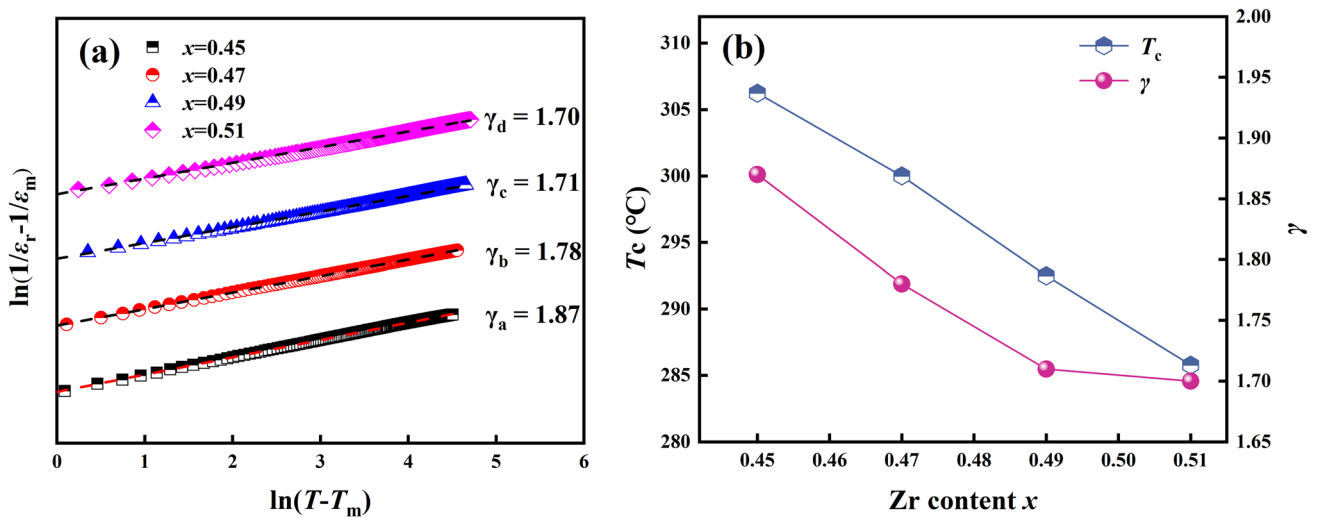


Fig. 7 (a) $\ln(1/\epsilon_r - 1/\epsilon_m)$ versus $\ln(T - T_m)$ curves for the 0.7PZTx-0.3PZN piezoceramics with different Zr content measured at 1 kHz. (b) Diffuseness degree (γ) and Curie temperature (T_c) for the piezoceramics with various Zr content.

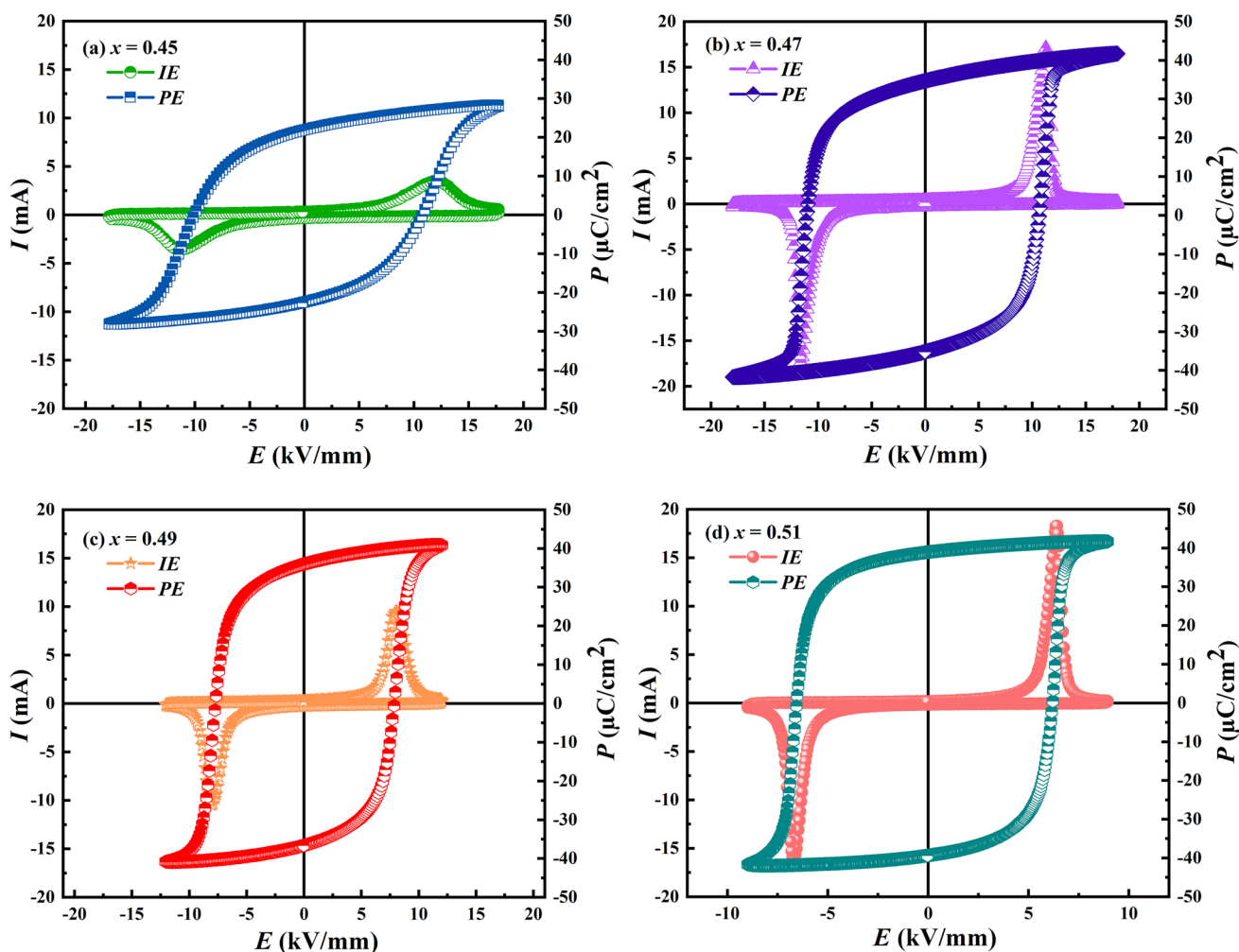


Fig. 8 Polarization–electric field (P – E) hysteresis loops and current–electric field (I – E) of $0.7\text{PZT}_x\text{-}0.3\text{PZN}$ piezoceramics. (a) $x=0.45$, (b) $x=0.47$, (c) $x=0.49$, (d) $x=0.51$.

ceramics to achieve enhanced piezoelectric properties. XRD analyses showed that the ceramic phase structure shifted from tetragonal phase-dominated to rhombohedral phase with increasing Zr content. A Gaussian fitting curve was used to separate the diffraction peaks representing the tetragonal and rhombohedral phases, and it was determined that the MPB was located between $x=0.49$ and 0.51 . Significantly enhanced piezoelectric, dielectric, and ferroelectric properties were located at $x=0.49$, with about 32% tetragonal and 68% rhombohedral phases in the phase structure. In addition, $0.7\text{PZT}_x\text{-}0.3\text{PZN}$ ceramics maintained high electrical properties at higher Curie temperatures: $T_c = 292.5^\circ\text{C}$, $d_{33} = 483$ pC/N, and $k_p = 0.69$. Our study provides insights into tuning the Zr content in the $0.7\text{PbZr}_x\text{Ti}_{1-x}\text{O}_3\text{-}0.3\text{Pb}(\text{Zn}_{1/3}\text{Nb}_{2/3})\text{O}_3$ system to build MPBs to enhance piezoelectric properties, and studying the effects of these phase transitions and phase boundaries

on the material properties can help to gain insights into the origins of their piezoelectric properties. Since the ability to improve the piezoelectric properties of ceramics based on compositional modulation is limited, it can be followed up by experimental studies of doping modifications.

Acknowledgments This work was supported by the Postgraduate Research & Practice Innovation Program of Yancheng Institute of Technology (SJCX22_XZ001), the funding for school-level research projects of Yancheng Institute of Technology (No. xjr2021016, xj201528), the major technological research in Lianyungang City unveiled the list of marshal projects (No. CGJBS2202), and the funding for post-doctoral research of Lianyungang City (No. 202012). The authors are grateful to the Lianyungang Advanced Ceramics and Structures Engineering Technology Research Centre for their assistance.

Data Availability All data generated or analyzed during this study are included in this published article.

Conflict of interest There is no conflict of interest to declare.

Consent to Publish All authors agree to publish in the Journal of Electronic Materials.

References

- H. Lu, H. Cui, G. Lu, L. Jiang, R. Hensleigh, Y. Zeng, A. Rayes, M.K. Panduranga, M. Acharya, Z. Wang, A. Irimia, F. Wu, G.P. Carman, J.M. Morales, S. Putterman, L.W. Martin, Q. Zhou, and X. Zheng, 3D Printing and processing of miniaturized transducers with near-pristine piezoelectric ceramics for localized cavitation. *Nat. Commun.* 14(1), 2418 (2023).
- D. Zhu, Z. Lai, and Z. Wang, Freeze–thaw process of soil between two piles as monitored by piezoelectric ceramic sensor. *Sci. Rep.* 13(1), 5706 (2023).
- X. Lin, X. Zhang, X. Fei, C. Wang, H. Liu, and S. Huang, Flexible three-dimensional interconnected PZT skeleton based piezoelectric nanogenerator for energy harvesting. *Ceram. Int.* 49(16), 27526–27534 (2023).
- Q. Chi, L. Xu, C. Zhang, Y. Zhang, Y. Zhang, C. Tang, and T. Zhang, Enhancing the high-temperature energy storage performance of PEI dielectric film through deposition of high-dielectric PZT coating layer. *Ceram. Int.* 49(16), 26246–26255 (2023).
- C. Chen, R. Liang, Z. Zhou, W. Zhang, and X. Dong, Enhanced bipolar fatigue resistance in PMN–PZT ceramics prepared by spark plasma sintering. *Ceram. Int.* 44(4), 3563–3570 (2018).
- Q. Guo, F. Li, F. Xia, X. Gao, P. Wang, H. Hao, H. Sun, H. Liu, and S. Zhang, High-Performance Sm-Doped Pb(Mg_{1/3}Nb_{2/3})O₃-PbZrO₃-PbTiO₃-Based Piezoceramics. *ACS Appl. Mater. Interfaces* 11(46), 43359–43367 (2019).
- K. Wen, J. Qiu, H. Ji, K. Zhu, J. Liu, J. Wang, J. Du, and F. Zhu, Investigation of phase diagram and electrical properties of xPb(Mg_{1/3}Nb_{2/3})O₃-(1-x)Pb(Zr_{0.4}Ti_{0.6})O₃ ceramics. *J. Mater. Sci. Mater. Electron.* 25(7), 3003–3009 (2014).
- J. Yan, Y. Hou, X. Yu, M. Zheng, and M. Zhu, Large enhancement of transduction coefficient in PZN–PZT energy harvesting system through introducing low-er PIN relaxor. *J. Eur. Ceram. Soc.* 39(8), 2666–2672 (2019).
- H. Chen, T. Pu, Y. Luo, S. Fan, Q. Chen, H. Liu, and J. Zhu, Enhancement of piezoelectric properties in low-temperature sintering PZN–PZT ceramics by Sr²⁺ substitution. *J. Electron. Mater.* 51(3), 1261–1271 (2022).
- G.F. Fan, M.B. Shi, W.Z. Lu, Y.Q. Wang, and F. Liang, Effects of Li₂CO₃ and Sm₂O₃ additives on low-temperature sintering and piezoelectric properties of PZN–PZT ceramics. *J. Eur. Ceram. Soc.* 34(1), 23–28 (2014).
- L. Bian, X. Qi, K. Li, J. Fan, Z. Li, E. Sun, B. Yang, S. Dong, and W. Cao, High-performance Pb(Ni_{1/3}Nb_{2/3})O₃-PbZrO₃-PbTiO₃ ceramics with the triple point composition. *J. Eur. Ceram. Soc.* 41(14), 6983–6990 (2021).
- F. Guo, S. Zhang, W. Long, P. Fang, X. Li, and Z. Xi, SnO₂ modified PNN–PZT ceramics with ultra-high piezoelectric and dielectric properties. *Ceram. Int.* 48(16), 23241–23248 (2022).
- T. Pu, H. Chen, J. Xing, Y. Luo, S. Fan, H. Liu, Q. Chen, and J. Zhu, High piezoelectricity of low-temperature sintered Li₂CO₃-added PNN–PZT relaxor ferroelectrics. *J. Mater. Sci. Mater. Electron.* 33(8), 4819–4830 (2022).
- G.G. Peng, D.Y. Zheng, C. Cheng, J. Zhang, and H. Zhang, Effect of rare-earth addition on morphotropic phase boundary and relaxation behavior of the PNN–PZT ceramics. *J. Alloy. Compd.* 693, 1250–1256 (2017).
- A. Kumar, A.K. Kalyani, R. Ranjan, K.C.J. Raju, J. Ryu, N. Park, and A.R. James, Evidence of monoclinic phase and its variation with temperature at morphotropic phase boundary of PLZT ceramics. *J. Alloy. Compd.* 816, 152613 (2020).
- H. Wang, F. Zhang, Y. Chen, C. Huang, X. Wang, X. Wu, Y. Chen, Y. Xu, S. Guan, J. Zhu, Q. Chen, and J. Xing, Giant piezoelectric coefficient of PNN–PZT-based relaxor piezoelectric ceramics by constructing an R-T MPB. *Ceram. Int.* 47(9), 12284–12291 (2021).
- V. Tiwari, and G. Srivastava, The effect of Li₂CO₃ addition on the structural, dielectric and piezoelectric properties of PZT ceramics. *Ceram. Int.* 41(2), 2774–2778 (2015).
- H.L. Wang, F.F. Zhang, Y. Chen, C.T. Huang, X.Y. Wang, X.J. Xu, Y.L. Chen, Y.G. Xu, S.Y. Guan, J.G. Zhu, Q. Chen, and J. Xing, Giant piezoelectric coefficient of PNN–PZT-based relaxor piezoelectric ceramics by constructing an R-T MPB. *Ceram. Int.* 47(9), 12284–12291 (2021).
- Y.X. Guo, W.B. Ma, and F. Zhang, The effect of PSN content on MPB of 0.3Pb(Ni_{1/3}Nb_{2/3})O₃-0.7Pb(Zr_{1-x}Tx)O₃ system. *J. Mater. Sci. Mater. Electron.* 27, 1520–1527 (2016).
- J.B. Zhang, H. Liu, S.D. Sun, Y. Liu, Y.Y. Zhang, H. Qi, S.Q. Deng, and J. Chen, Crystal structure and actuation mechanisms in morphotropic phase boundary Pb(Zn_{1/3}Nb_{2/3})O₃-Pb(Zr_{1/2}Ti_{1/2})O₃ piezoelectric ceramic. *J. Am. Ceram. Soc.* 104(6), 2621–2627 (2021).
- H.L. Li, Y. Zhang, J.J. Zhou, X.W. Zhang, H. Liu, and J.Z. Fang, Phase structure and electrical properties of xPZN-(1-x)PZT piezoceramics near the tetragonal/rhombohedral phase boundary. *Ceram. Int.* 41(3), 4822–4828 (2015).
- N. Vittayakorn, G. Rujjanagul, X. Tan, H. He, M.A. Marquardt, and D.P. Cann, Dielectric properties and morphotropic phase boundaries in the xPb(Zn_{1/3}Nb_{2/3})O₃-(1-x)Pb(Zr_{0.5}Ti_{0.5})O₃ pseudo-binary system. *J. Electroceram.* 16(2), 141–149 (2006).
- A.M. Geetika, Umarji, The influence of Zr/Ti content on the morphotropic phase boundary in the PZT–PZN system. *Mater. Sci. Eng. B* 167(3), 171–176 (2010).
- N. Wang, Q. Sun, W. Ma, Y. Zhang, and H. Liu, Investigation of La-doped 0.25Pb(Zn_{1/3}Nb_{2/3})O₃-0.75Pb(ZrxTi_{1-x})O₃ ceramics near morphotropic phase boundary. *J. Electroceram.* 28(1), 15–19 (2012).
- Z.Q. Zeng, Q.C. Wu, M.M. Hao, W.Z. Lu, G.F. Fan, M.Y. Chi, and M.Y. Ding, Impedance spectroscopy and piezoelectric property of LiF-doped PZN–PZT low-temperature sintering piezoelectric ceramics. *J. Mater. Sci. Mater. Electron.* 29, 8279–8286 (2018).
- M. Zheng, Y. Hou, M. Zhu, M. Zhang, and H. Yan, Shift of morphotropic phase boundary in high-performance fine-grained PZN–PZT ceramics. *J. Eur. Ceram. Soc.* 34(10), 2275–2283 (2014).
- H. Liu, J. Chen, L. Fan, Y. Ren, Z. Pan, K.V. Lalitha, J. Rödel, and X. Xing, Critical role of monoclinic polarization rotation in high-performance perovskite piezoelectric materials. *Phys. Rev. Lett.* 119, 017601 (2017).
- M. Promsawat, A. Watcharapasorn, Z.G. Ye, and S. Jiansiri-somboon, Enhanced dielectric and ferroelectric properties of Pb(Mg_{1/3}Nb_{2/3})_{0.65}Ti_{0.35}O₃ ceramics by ZnO modification. *J. Am. Ceram. Soc.* 98(3), 848–854 (2015).
- Y. Chen, H. Zhou, S. Wang, Q. Chen, Q. Wang, and J. Zhu, Diffused phase transition, ionic conduction mechanisms and electric-field dependent ferroelectricity of Nb/Ce co-doped Pb(Zr_{0.52}Ti_{0.48})O₃ ceramics. *J. Alloys Compd.* 854, 155500 (2021).
- H. Liu, R. Nie, Y. Yue, Q. Zhang, Q. Chen, J. Zhu, P. Yu, D. Xiao, C. Wang, and X. Wang, Effect of MnO₂ doping on piezoelectric, dielectric and ferroelectric properties of PNN–PZT ceramics. *Ceram. Int.* 41(9), 11359–11364 (2015).

31. L. Tang, X. Zhou, M. Habib, J. Zou, X. Yuan, Y. Zhang, and D. Zhang, Phase structure and electrical properties of BiFeO₃-BaTiO₃ ceramics near the morphotropic phase boundary. *Ceram. Int.* 49(19), 31965–31974 (2023).

Springer Nature or its licensor (e.g. a society or other partner) holds exclusive rights to this article under a publishing agreement with the author(s) or other rightsholder(s); author self-archiving of the accepted manuscript version of this article is solely governed by the terms of such publishing agreement and applicable law.

Publisher's Note Springer Nature remains neutral with regard to jurisdictional claims in published maps and institutional affiliations.